Journal of Energy Storage 130 (2025) 117470

Contents lists available at ScienceDirect

Journal of Energy Storage

journal homepage: www.elsevier.com/locate/est

Research papers

Preparation and performance characterisation of a physically and chemically crosslinked self-healing phase change material

Jinbao Zhong, Jian Zhang *, Yongpeng Wang, Haoxi Fan, Xiangyi Meng, Xianglong Feng, Jianhang Yan

School of Mechanical Engineering, Inner Mongolia University of Science and Technology, Baotou, Inner Mongolia 014010, China

ARTICLE INFO

Keywords:
Phase change materials
Polyurethane
Polyethylene glycol
Self-healing
Expanded graphite

ABSTRACT

This paper addresses the leakage, low thermal conductivity, low enthalpy, structural instability and difficult recovery problems associated with traditional polyethylene glycol (PEG)-based polyurethane phase change materials (PCMs). To this end, a multi-scaffold flexible composite phase change material (DS-FCPCM) was prepared via a combination of physical adsorption and chemical bonding. Structurally, expanded graphite-silica sol was employed as the physical adsorption scaffold, diphenylmethane diisocyanate (MDI) as the hard segment of the chemical cross-linking scaffold, and butanedione dioxime (DMG) as a chain extender to achieve PEG encapsulation. The study revealed that the thermal conductivity of DS-FCPCM measured 1.81 times higher than that of pure PEG. Following 200 thermal cycles, the material exhibited consistent heat storage capacity relative to its initial state without any leakage. The incorporation of DMG facilitated the formation of oxime-urethane bonds, a class of dynamic covalent bonds, which endowed the material with fracture-healing capabilities. extending its service life while reducing maintenance costs. Furthermore, heating and cooling experiments verified the thermal regulation ability of DS-FCPCM in practical applications. The results showed that the thermal response rate of the DS-FCPCM sample was 2.11 times that of pure PEG, and the maximum temperature difference of the system at the same time was 8.1 °C. This work provides a new approach to improving the heat storage performance of polyurethane PCMs, and is of great significance for the development of reworkable and environmentally friendly energy storage materials.

1. Introduction

With the continuous growth of global energy demand and the increasingly severe issue of resource scarcity, the development of efficient energy storage technologies has become a crucial pathway towards achieving sustainable development [1]. Phase change materials (PCMs), owing to their high energy storage density and stable thermal regulation capabilities, demonstrate unique advantages in the field of thermal management [2]. Research indicates that thermal management technologies incorporating PCMs have been successfully applied in solar thermal storage [3], battery thermal management [4], building insulation [5], thermal protection of electronic devices [6], and waste heat recovery [7]. Notably, organic solid-liquid PCMs such as polyethylene glycol (PEG) [8] and paraffin [9] have gained widespread use due to their high latent heat, suitable phase transition temperatures, cost-effectiveness, and low supercooling characteristics. Although their unique energy storage advantages demonstrate profound application potential [10], the low thermal conductivity, phase change leakage, structural fragility, and difficulty in recycling of solid-liquid PCMs themselves significantly limit their application in thermal management technologies [11]. Therefore, developing a composite phase change material with excellent heat storage properties and environmental safety is of paramount importance.

Research indicates that flexible composite phase change materials (FCPCMs) synthesised via chemical encapsulation methods can effectively address the leakage issues of PCMs during phase transition [12]. Common FCPCMs include ethylene-vinyl acetate [13], polyurethane [14], polydimethylsiloxane [15], thermoplastic resins [16], polyethylene [17], and polypropylene [18]. Among these, polyurethane-based phase change materials demonstrate significant advantages in thermal conductivity, leakage resistance, and mechanical strength compared to other FCPCMs. Polyurethane-encapsulated phase change

* Corresponding author at: Arding Street No.7, Inner Mongolia University of Science & Technology, Baotou 014010, China.
E-mail address: 2896510776@qq.com (J. Zhang).

https://doi.org/10.1016/j.est.2025.117470
Received 29 March 2025; Received in revised form 20 May 2025; Accepted 13 June 2025
Available online 17 June 2025
2352-152X/© 2025 Elsevier Ltd. All rights are reserved, including those for text and data mining, AI training, and similar technologies.

Table 1
Composition ratios of different samples.

Sample	PEG(wt %)	PEG:MDI:DPE:DMG(molar ratio)	EG(wt %)	SNOWTEX(wt %)
A1	82	1:4.30:0.78:0.12	1.2	2.2
A2	81	1:4.65:0.77:0.11	1.0	2.0
A3	80	1:5.00:0.76:0.10	1.4	2.4
B1	82	1:4.30:0.78:0.12	0	0
B2	81	1:4.65:0.77:0.11	0	0
B3	80	1:5.00:0.76:0.10	0	0

materials have been widely applied in intelligent thermoregulatory textiles, renewable energy and industrial thermal storage systems, building energy efficiency and temperature-control materials, medical and specialised functional materials, and thermal management of flexible electronic devices. Liu et al. [19] synthesised polyurethane microencapsulated phase change materials through in situ polymerisation, which exhibited exceptional thermal stability, cycling durability, and high energy storage efficiency. Zhou et al. [20] developed a hyperbranched waterborne polyurethane solid-solid phase change material, demonstrating its high feasibility and application potential in intelligent thermoregulatory textile industries. Despite the advantages of polyurethane materials over other FCPCMs, they still exhibit lower thermal conductivity and greater environmental susceptibility compared to traditional physical encapsulation materials, potentially leading to material waste and environmental pollution [21]. Consequently, increasing research efforts are dedicated to developing polyurethane phase change materials with superior thermal performance.

Inspired by molecular dynamics, the incorporation of dynamic bonds into polyurethane structures has emerged as a pivotal strategy to confer reversible reconfiguration capabilities upon materials [22]. This approach synergistically leverages temperature and pressure variations during phase transitions to achieve self-healing functionality, thereby addressing structural vulnerability issues. Numerous dynamic bonds compatible with polyurethane polymerisation reactions have been explored, including Diels-Alder bonds [23,24], disulfide bonds [25,26], diselenide bonds [27,28], Schiff base bonds [29,30], oxime-carbamate bonds [31,32], and phenol-carbamate bonds [33,34]. Among these, oxime-carbamate bonds offer distinctive advantages for polymer material science applications due to their high reversibility, multi-reactivity, dynamic characteristics, robust chemical stability, and potential for facile synthesis and modification. Xu et al. [35] synthesised cross-linked network polyurethanes with varying crosslinking densities, achieving outstanding self-healing properties (97 % recovery) and reprocessibility via oxime-carbamate bond interactions. Wang et al. [36] developed a self-healing polyurethane elastomer incorporating dynamic oxime-carbamate bonds, demonstrating a healing efficiency of 101 % at 70 °C. However, critical analysis of existing literature reveals limited exploration of oxime-carbamate bonds in polyurethane phase change materials (PCMs), with composite performance parameters, particularly thermal conductivity, remaining suboptimal compared to those of conventional PCMs.

Traditional physical encapsulation technology confines phase change materials (PCMs) within porous matrices or 3D networks to produce stable composite PCMs, a methodology that has been proven effective in enhancing thermal conductivity. Representative encapsulation materials encompass silica aerogels [37,38], bentonite [39,40], and activated carbon [41,42]. Among these, expanded graphite (EG) has been extensively used as an economically viable, readily available, and highly thermally conductive porous material for the preparation of composite PCMs. Jia et al. [43] developed a composite PCM incorporating hydrophilically modified EG as a high-thermal-conductivity additive, which demonstrated a 71 % enhancement in thermal conductivity compared to the pristine PCM. Zhao et al. [44] employed EG in combination with low-melting-point metal-based alloys for PCM encapsulation, achieving a thermal conductivity of 2.31 W/(m·K). However, the inherent weak compatibility between EG and solid-liquid PCMs frequently induces agglomeration during composite fabrication, thereby limiting the overall thermal energy storage performance. Silica sol, comprising amorphous SiO_2 colloidal particles, presents an alternative encapsulation material that not only improves the thermal conductivity of the composite but also exhibits superior compatibility with conventional PCMs. Yan et al. [45] synthesised a composite material utilising aminopropyl-functionalised silica networks, which attained enhanced thermal conductivity (0.421 W/(m·K)) and favourable shape stability. Wang et al. [46] fabricated polyethylene glycol (PEG)-based shape-stabilized PCMs using silica microspheres as mesoporous matrices, where the microspheres not only reinforced shape stability but also established defined heat transfer pathways. Nevertheless, the amorphous nature of these structures inherently compromises mechanical stability in resultant composites. This dichotomy between enhanced thermal performance and structural integrity underscores the critical need for developing composite thermal management systems that harmonise mechanical robustness and material compatibility.

Consequently, we have successfully synthesised a physicochemically cross-linked flexible composite phase change material (DS-FCPCM) exhibiting high thermal conductivity, structural stability, and self-healing capabilities. Firstly, using polyethylene glycol (PEG) as the thermal energy storage matrix, a polyurethane chemical encapsulation network was constructed with diphenylmethane diisocyanate (MDI). Notably, dimethylglyoxime (DMG) and dipentaerythritol (DPE) were introduced as dynamic chain extenders to establish an oxime-carbamate dynamic covalent bond architecture. Subsequently, physical encapsulation was synergistically integrated via the development of a dual-structure (DS) scaffold combining expanded graphite (EG) and silica sol. This DS architecture achieves complementary enhancement of the mechanical stability of EG and the phase compatibility of silica sol. Crucially, chemical bonding between hydroxyl groups on the silica sol surface and isocyanate groups within the polyurethane matrix facilitates two thermal conduction pathways: interlayer heat transfer through EG platelets and network-based conduction via silica sol bridges. This multiscale composite strategy endows the DS scaffold with structural integrity and continuous thermal transport, thus providing innovative thermal management support for flexible PCMs. Material characterisation reveals exceptional performance metrics for DS-FCPCM: a thermal conductivity of 0.5023 W/(m·K), an enthalpy of 91.724 J/g, a fracture stress of 12.9 MPa, an elongation at break of 954 %, and a healing efficiency of 89.14 %. These parameters collectively demonstrate the material's superior thermal storage capacity, mechanical resilience, and self-healing functionality. Furthermore, accelerated thermal cycling tests (200 cycles) substantiate the material's potential for practical thermal management applications. This research not only establishes a novel pathway for enhancing polyurethane-based PCM performance but also holds significant implications for developing sustainable energy storage materials aligned with green low-carbon initiatives.

2. Materials and methods

2.1. Materials

Polyethylene glycol 4000 (PEG4000, Mn = 4000 Da), Sinopharm Chemical Reagent Co Ltd. (China); silica sol (SNOWTEX), Shandong Yousuo Chemical Technology Co., Ltd. (China); expanded graphite (EG), Nanjing Greifei Carbon Materials Co., Ltd. (China); dibutyltin dilaurate (DBTDL), dipentaerythritol (DPE), tetrahydrofuran (THF), dimethylglyoxime (DMG), 3-aminopropyltriethoxysilane (KH550), Shanghai Macklin Biochemical Co., Ltd. (China); *N*,*N*-dimethylformamide (DMF), Shanghai Aladdin Biochemical Technology Co., Ltd. (China); diphenylmethane diisocyanate (MDI), Wanhua Chemical Group Co., Ltd. (China). Before the experiment, MDI, EG, and PEG were dehydrated using 5 Å molecular sieves for 10 days.

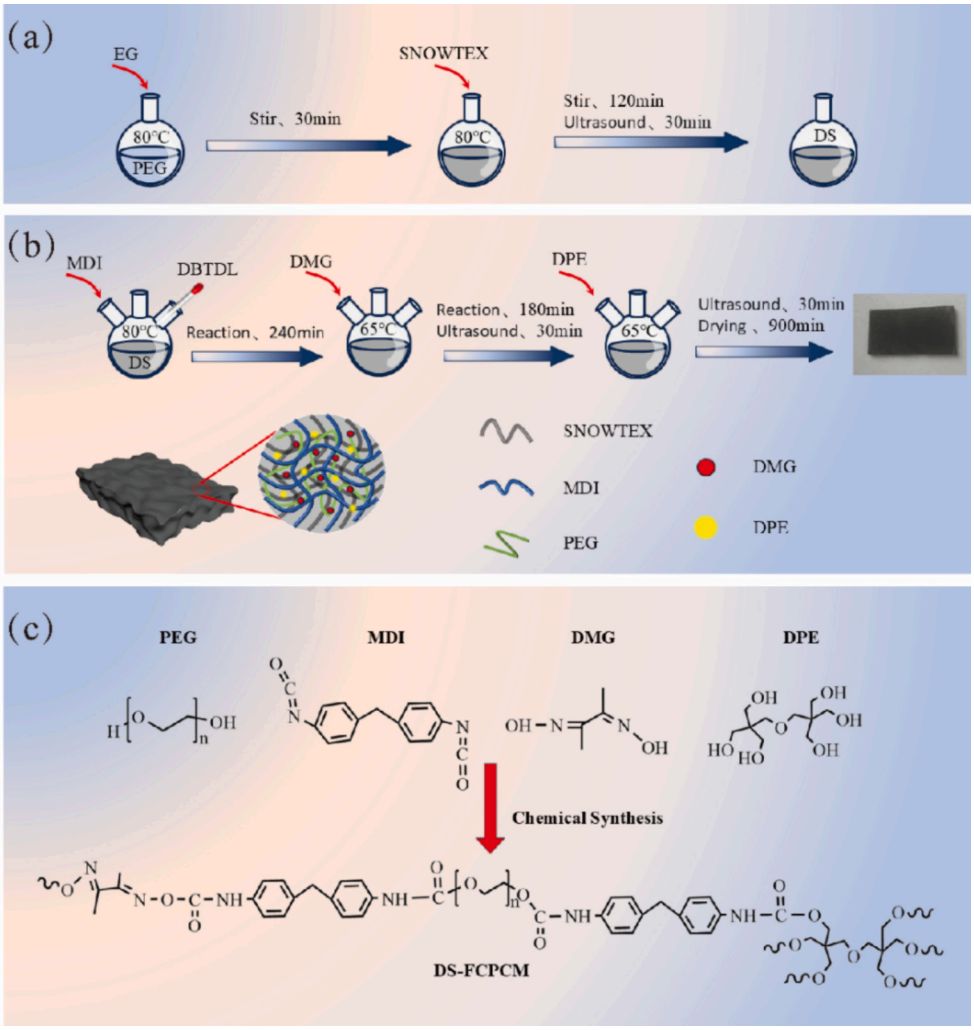

Fig. 1. (a) Experimental flow chart; (b) Schematic diagram of chemical bonding.

2.2. Material preparation

2.2.1. Preparation of the DS skeleton

The DS skeleton was prepared according to the material proportions outlined in Table 1. As shown in Fig. 1(a), graphite that had been dried for 5 h was removed and placed in a muffle furnace at 900 °C for 1 min to obtain dried, expanded graphite. Dried PEG was then vacuum-heated to 80 °C. Subsequently, the prepared expanded graphite and a silica sol solution were added to a beaker. Simultaneously, KH550 (5 % of the silica sol mass) was hydrolysed for 5 min and added to the beaker. The mixture was stirred at 80 °C for 2 h and then sonicated in a CNC ultrasonic cleaner for 30 min, resulting in the DS solution.

2.2.2. DS-FCPCM preparation

The DS-FCPCM was prepared according to the material proportions outlined in Table 1. As shown in Fig. 1(b), MDI was completely dissolved in DMF, and this solution was poured into a beaker containing the DS. Next, 3 drops of DBTDL were added as a catalyst, and the mixture was heated to 80 °C and reacted for 4 h. After this, the temperature was reduced to 65 °C, and a DMG solution dissolved in an appropriate amount of THF was added. Subsequently, the mixture was placed in a CNC ultrasonic cleaner at the same temperature and sonicated for 30 min. Following sonication, the reaction was continued at 65 °C for 3 h. A DPE solution dissolved in an appropriate amount of DMF was added to the mixture, and it was again placed in the CNC ultrasonic cleaner for 30 min to ensure the solution was mixed thoroughly. Finally, the mixture was poured into a polytetrafluoroethylene mould and dried in a fan-assisted drying oven for 15 h to obtain the DS-FCPCM sample. As shown in Fig. 1(c), in the reaction between MDI and PEG, the hydroxyl groups at both ends of the PEG molecular chain acted as nucleophiles, attacking the carbon atoms in the isocyanate groups of MDI, resulting in a nucleophilic addition reaction. Based on the characteristics of the polymerisation reaction, PEG6000, MDI, dipentaerythritol, and butanedione dioxime were reacted according to different monomer molar ratios to obtain samples A1, A2, and A3, and samples B1, B2, and B3 without the DS scaffold. Samples A1, A2, and A3 were thermally cycled 200 times to obtain samples C1, C2, and C3.

2.3. Characterisation methods

The material structure was characterised using Fourier transform infrared spectroscopy (FTIR) and X-ray diffraction (XRD). FTIR testing was performed using an infrared spectrometer (Thermo Fisher Scientific Nicolet iS20, USA), primarily to determine the chemical structure and composition of the substance, identify specific functional groups in the molecule, and determine the types of groups in the molecule by analysing characteristic absorption frequencies. XRD testing was performed using an X-ray diffractometer (Rigaku SmartLab SE, Japan), where the sample was irradiated with X-rays at a scanning speed of 2°/min over an angular range of 0–90°, and the resulting diffraction phenomena in the sample crystal were observed and recorded for crystal structure analysis.

The phase transition characteristics of the material were investigated

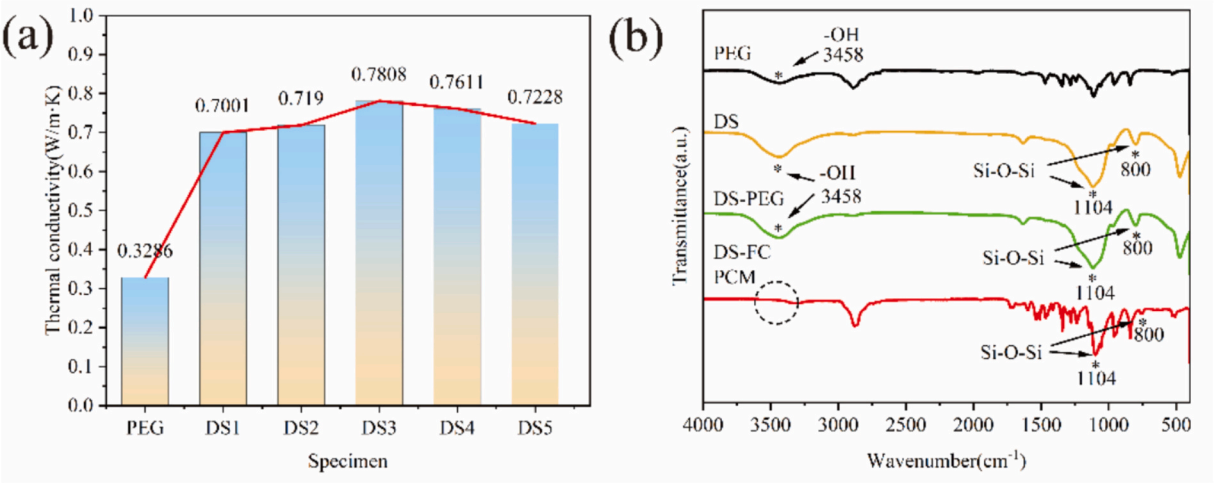

Fig. 2. (a) Bar chart of thermal conductivity for DS with different compositional ratios; (b) Fourier transform infrared (FTIR) spectra of PEG, DS, DS-PEG, and DS-FCPCM.

Table 2
Compositional ratios of different DS samples.

Sample	PEG(wt%)	EG(wt%)	SNOWTEX(wt%)	KH550(wt%)
DS1	96.90	1.0	2.0	0.10
DS2	96.68	1.0	2.2	0.11
DS3	96.49	1.2	2.2	0.11
DS4	96.28	1.2	2.4	0.12
DS5	96.08	1.4	2.4	0.12

using differential scanning calorimetry (DSC, TA Q20, USA) to accurately determine the material's melting point, crystallisation temperature, and heat storage/release enthalpy values under a nitrogen atmosphere. Thermal conductivity was measured using a thermal constants analyser (TP2500S, Sweden) for rapid and accurate determination of the material's thermal conductivity. Thermal stability was analysed using thermogravimetric analysis (TGA 550, TA Instruments, USA) to determine the material's thermal stability and compositional changes under a nitrogen atmosphere from 30 °C to 800 °C. Leaking experiments, MDI tolerance experiments, hot pressing experiments, tensile test and water bath experiments were designed to verify the material's physical and heat storage properties, thereby providing a scientific basis for material research and development, and quality control.

3. Results and discussion

3.1. DS skeleton structure

To optimise the thermal energy storage performance of DS-FCPCM, this study investigated the influence of silica sol/EG composite ratios on the material's thermal conductivity. Characterisation was performed using a thermal constant analyser and Fourier transform infrared (FTIR) spectroscopy. Fig. 2(a) shows the thermal conductivity variation of DS samples with different compositional ratios. Increasing the mass proportion of silica sol initially increased thermal conductivity (DS2 showed a 2.7 % enhancement compared to DS1), indicating a direct proportional relationship at this stage. Further increasing the mass proportion of expanded graphite (EG) also increased thermal conductivity (DS3 demonstrated an 8.5 % improvement compared to DS2). These findings demonstrate that EG plays a dominant role in enhancing the thermal conductivity of the DS structure. However, exceeding 2.2 wt % silica sol (DS4 showed a 2.5 % decline compared to DS3) or 1.4 wt% EG (DS5 exhibited a 5 % reduction compared to DS4) induced interfacial thermal resistance, decreasing thermal performance. The DS3 formulation achieved the highest thermal conductivity (0.7808 W/(m·K)); specific ratios are detailed in Table 2.

Fig. 2(b) shows the Fourier transform infrared images of PEG, DS, DS-PEG, and DS-FCPCM. The peak observed at 3458 cm^{-1} in the DS-PEG curve results from the overlapping of the Si-OH groups on the silica sol,

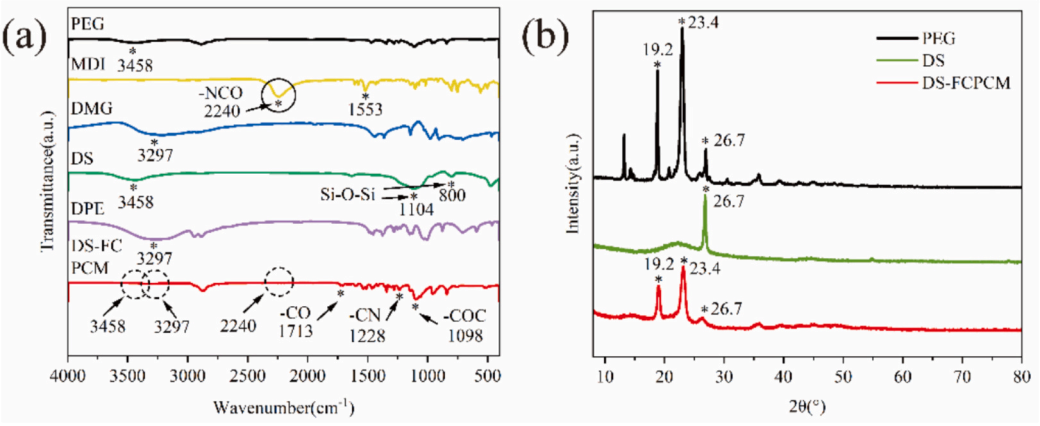

Fig. 3. (a) Fourier transform infrared spectra of PEG, MDI, DS, DMG, DPE, and DS-FCPCM;
(b) XRD spectra of PEG, DS, and DS-FCPCM.

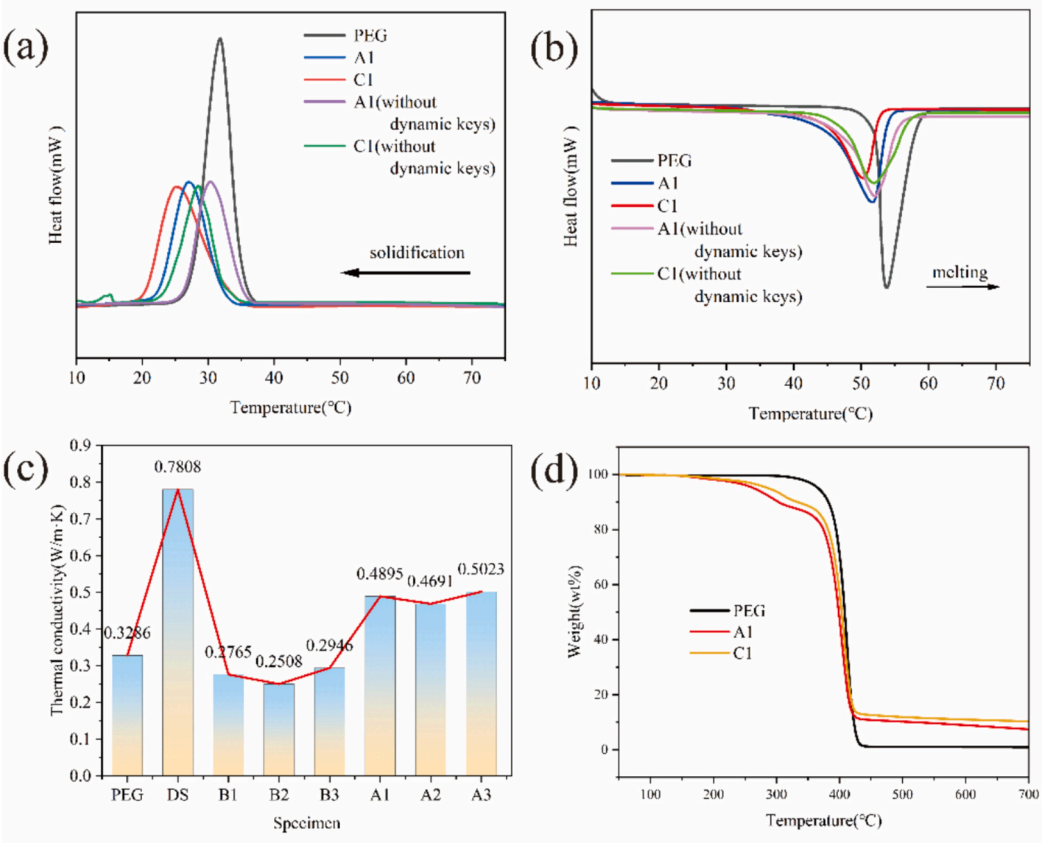

Fig. 4. (a) DSC curves for heat release of samples; (b) DSC curves for heat absorption of samples; (c) Bar chart of thermal conductivity of samples; (d) TG curves of samples.

Table 3
Summary table of key parameters for several polyurethane phase change materials.

Sample	Endothermic Temperature (°C)	Exothermic Temperature (°C)	Endothermic Enthalpy (J/g)	Exothermic Enthalpy (J/g)	Enthalpy Loss Rate Before and After Cycling	Ref
PTPCM-R	52.70	20.70	79.80	72.00	–	[12]
DOU-PUPCMs	47.90	18.60	72.90	68.62	–	[21]
PUP-N	50.10	16.30	70.99	72.27	12.8 % (100 cycles)	[47]
PTMEG	21.90	8.50	92.80	94.30	0.8 % (20 cycles)	[48]
Cu2 + -OUPCMs	52.70	22.70	81.83	85.65	–	[49]
DS-FCPCM	50.27	27.06	91.72	81.65	1.8 % (200 cycles)	This work

the -OH groups on the EG, and the -OH groups on the PEG, indicating that EG is physically connected to the silica sol through the adsorption effect of the EG. However, no comparable -OH peak is detected at 3458 cm^{-1} in the DS-FCPCM curve, suggesting that the -OH groups in DS and PEG have chemically bonded with the -NCO groups on MDI, forming a tightly integrated composite structure. The peaks observed at 1104 and 800 cm^{-1} correspond to the vibrations of Si-O-Si bonds generated by the condensation reaction of Si-OH groups in the silica sol, with similar vibrational peaks also found at the same positions in the DS-FCPCM curves. The results indicate that the connection between DS and the phase change colloid involves both physical and chemical interactions. In summary, a three-dimensional thermally conductive structure that combines interlayer conduction (EG) and longitudinal network conduction (silica sol) has been successfully synthesised in the structure of DS-FCPCM. Furthermore, the strong physical adsorption properties of EG enable a close connection between DS and the DS-FCPCM phase change material, resulting in a thermally conductive phase change material characterised by a complex interplay of physical and chemical bonding.

3.2. Chemical structure

The chemical structures of PEG, DS, MDI, DMG, DPE, and DS-FCPCM were characterised using FTIR spectroscopy. In Fig. 3(a), the MDI spectrum exhibited a characteristic peak at 2240 cm^{-1} corresponding to -NCO group vibrations, while the peak at 1553 cm^{-1} arose from aromatic C═C stretching in its benzene ring structure. Peaks observed at 3458 and 3297 cm^{-1} in the spectra of other materials were attributed to -OH group vibrations. Notably, the DS-FCPCM spectrum did not show these characteristic peaks at 2240, 3458, and 3297 cm^{-1}, but displayed new vibrational bands at 1713 cm^{-1} (C═O stretching), 1228 cm^{-1} (C—N stretching), and 1098 cm^{-1} (C-O-C stretching). This spectral evolution confirms the successful consumption of hydroxyl groups (-OH) through complete reaction with -NCO groups from MDI, resulting in urethane (-NH-COO-) formation. The findings demonstrate MDI's complete conversion and successful synthesis of polyurethane phase-change

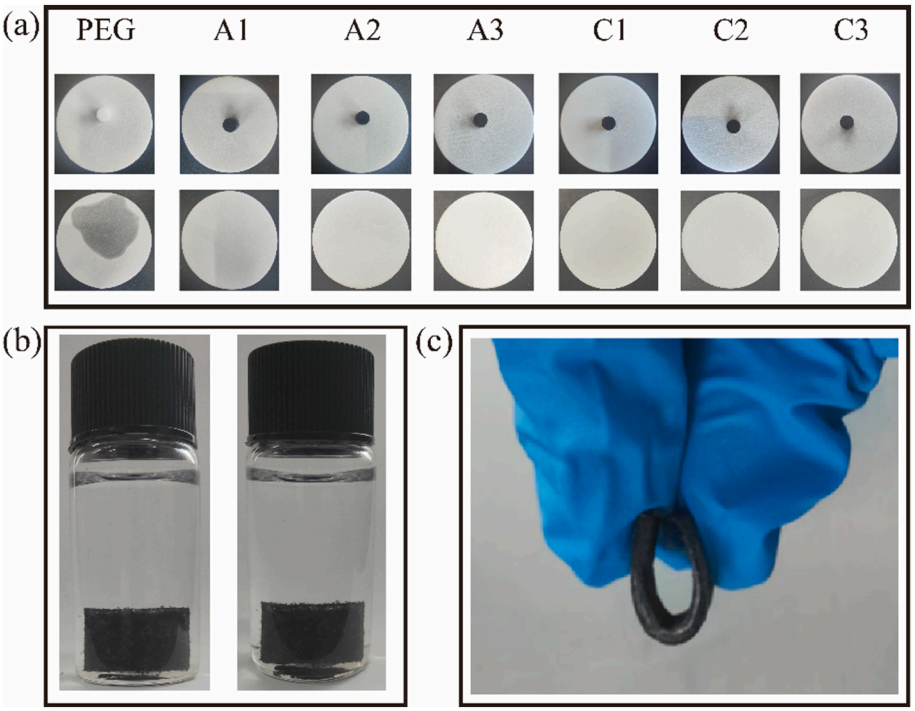

Fig. 5. (a) Leakage experiment; (b) Digital images of solvent immersion; (c) Digital images of samples under flexural stress.

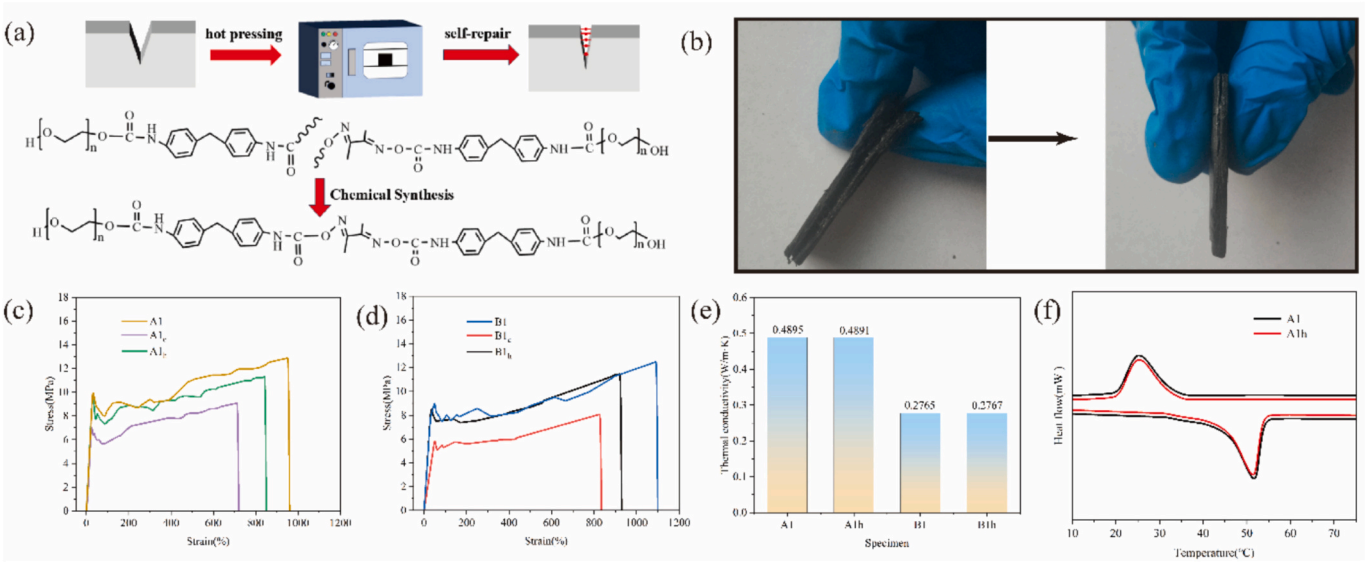

Fig. 6. (a) Schematic diagram of thermal healing experiment; (b) Comparative photograph of thermal healing experiment; (c) Stress-strain curves of sample A1 under different healing states; (d) Stress-strain curves of sample B1 under different healing states. (e) Bar chart of thermal conductivity before and after sample healing; (f) DSC curve of sample A1 before and after healing.

Table 4
Summary of key mechanical performance parameters for several self-healing materials.

Sample	Self-Healing Rate	Elongation (%)	Stress (MPa)	Ref
PTPCM-R	–	856.20 %	11.18	[12]
DOU-PUPCMs	80.00 %	998.16 %	14.55	[21]
PUP-N	–	486.44 %	11.96	[47]
SSPCM	91.04 %	625.00 %	–	[51]
DS-FCPCM	89.14 %	954.63 %	12.90	This work

material DS-FCPCM containing dynamic oxime-carbamate bonds.

Fig. 3(b) shows the XRD curves for PEG, DS, and DS-FCPCM. The diffraction peaks in the PEG curve at 2θ values of 19.2° and 23.4° correspond to its (120) and (032) crystal planes, respectively. In the DS curve, the diffraction peak at 2θ of 26.7° corresponds to the (002) crystal plane of EG. The DS-FCPCM curve shows diffraction peaks similar to those of both the PEG and DS curves, with essentially the same diffraction angles, diffraction lines, and interplanar spacings. This demonstrates that in the chemical long chain of DS-FCPCM, the soft segment PEG has a large molecular weight, leading to the same heat absorption and release behaviour during the phase transition. The diffraction peaks are smaller compared to those of PEG because the PEG

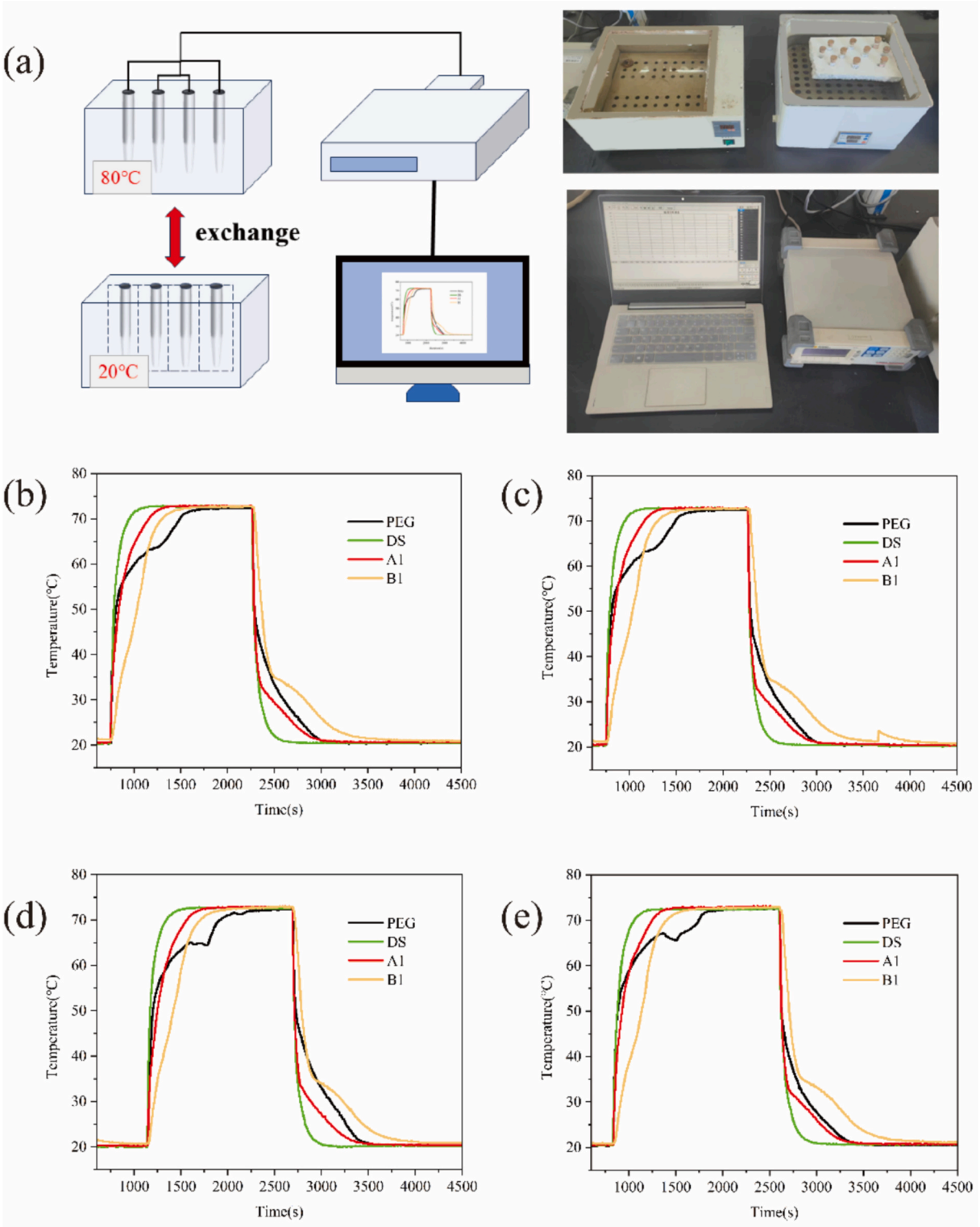

Fig. 7. (a) Schematic diagram of water bath experiment; (b) Temperature variation curves after 10 thermal cycles; (c) Temperature variation curves after 50 thermal cycles; (d) Temperature variation curves after 100 thermal cycles; (e) Temperature variation curves after 200 thermal cycles.

content is relatively low. At the same time, the dynamic oxime-urethane bonds generated by the reaction appear as hard segment impurities in the crystal structure, which also weakens the diffraction peaks. In addition, the addition of the DS thermally conductive network also hinders the crystallisation behaviour of the material's crystal structure, further limiting the crystallisation ability of DS-FCPCM.

3.3. *Thermal energy storage properties*

Differential Scanning Calorimetry (DSC) is a critical analytical technique for evaluating the thermal energy storage characteristics of materials. Fig. 4 (a) and 4(b) present the DSC curves for the exothermic and endothermic processes of PEG, A1, and C1 samples, respectively. The curves reveal that both A1 and C1, like PEG, exhibit excellent heat

Table 5
Summary table of temperature variation time for sample A1 under different cyclic conditions.

Sample	Heat-up time (s)	Cool-down time (s)	Maximum temperature difference (°C)
A1 (10 cycles)	516	785	8.10
A1 (50 cycles)	525	782	8.03
A1 (100 cycles)	522	771	8.01
A1 (200 cycles)	509	773	8.02

absorption and release capabilities. This similarity arises because the soft PEG segments within DS-FCPCM undergo crystallisation and melting processes in response to environmental temperature changes, mirroring the behaviour of pure PEG crystals. Minor supercooling is observed in the exothermic DSC curves of A1 and C1, attributed to the restricted crystallisation of PEG within the DS-FCPCM crosslinked network. Furthermore, compared to samples containing dynamic bonds, the phase transition temperature peaks of A1 and C1 (without dynamic bonds) are shifted to higher temperatures (by 11.6 %). This shift indicates that the presence of dynamic bonds partially inhibits crystallisation, materials without dynamic keys entered the exothermic stage earlier. In the endothermic DSC curves (Fig. 4 (b)), the peak absorption temperatures of A1 and C1 are lower than that of PEG, due to the enhanced thermal conductivity provided by the DS framework within the DS-FCPCM crosslinked network. Conversely, the absence of dynamic bonds increases the phase transition temperature (by 2.8 %), demonstrates that the presence of dynamic bonds reduces the thermal conductivity of the material, delays the material reaching its phase transition temperature. DS-FCPCM exhibits an exothermic enthalpy of 81.653 J/g and an endothermic enthalpy of 91.724 J/g. After 200 thermal cycles, the enthalpies remain stable at 80.114 J/g (exothermic) and 88.170 J/g (endothermic), indicating no degradation in thermal performance. In contrast, DS-FCPCM without dynamic bonds exhibits slightly lower enthalpies of 81.34 J/g (exothermic) and 92.004 J/g (endothermic). These results confirm that the incorporation of dynamic bonds reduces crystallisation capacity and the thermal conductivity of pure PEG without affecting enthalpy. Key parameters of existing polyurethane phase-change materials are summarised in Table 3.

To accurately measure thermal conductivity, the transient plane source method was employed. DS-FCPCM was compressed into cylindrical pellets (12 mm diameter) under 3 MPa pressure and analysed using a thermal constants analyser. As shown in Fig. 4(c), the chemically crosslinked polyurethane material exhibits a 15.8 % reduction in thermal conductivity compared to pure PEG. This reduction is attributed to the introduction of dynamic bonds, which hinder the inherent thermal pathways of PEG. However, the incorporation of a DS framework (thermal conductivity: 0.7808 W/(m·K)) increases the overall thermal conductivity by 181.67 %, reaching a maximum of 0.5023 W/(m·K). The conductivity increases proportionally with DS content, as the expanded graphite and silica sol within the DS framework form efficient thermal conduction channels, enhancing thermal performance while maintaining structural stability.

Fig. 4(d) shows continuous measurement images of the sample mass variation with temperature under programmed temperature control, representing the TG curves of PEG, A1, and C1. As can be seen from the images, the thermal decomposition range of PEG is 340–437 °C. The DS-FCPCM curve shows a peak at 325 °C, which is due to the sublimation of DMG. The second peak appears at 362 °C, which is related to the decomposition of urethane bonds. The third peak appears near 420 °C, corresponding to the thermal degradation of PEG. The specific thermal decomposition range of DS-FCPCM is 175–429 °C, far exceeding its operating range (10–120 °C), which does not affect its normal use. Sample C1, which has the same initial mass as A1 in the image, retains the same percentage of mass after thermal decomposition as before cycling, indicating that no leakage occurs in the DS-FCPCM during 200 cycles. The results show that the prepared DS-FCPCM has high thermal stability.

3.4. Physical properties

To assess the shape stability of the DS-FCPCM, leakage tests were conducted using cylindrical pellets of PEG, A1, A2, A3, C1, C2, and C3 samples (each with the same mass) compressed to a diameter of 12 mm, as shown in Fig. 5(a). The pellets were supported with filter paper and placed in a vacuum drying oven, maintained at 80 °C for 2 h. The mass of the samples was recorded before and after heating, and the mass loss was calculated. It was observed that the PEG pellet melted rapidly into a liquid upon heating, while the DS-FCPCM samples exhibited no leakage and remained completely encapsulated. This is because the presence of the DS scaffold, combined with the chemical cross-linked structure, causes the PEG crystals to be firmly locked in place when melting occurs, maintaining their original solid state even in environments above the phase transition temperature. This also indicates that the DS-FCPCM reacted successfully, forming a strong cross-linked network with good shape stability.

To test the solvent tolerance of the DS-FCPCM, rectangular slices of the material were immersed in DMF solvent, as shown in Fig. 5(b), and the state of the samples was recorded before and after 48 h. As can be seen in the images, the samples exhibited slight swelling after prolonged immersion but did not dissolve, indicating that the prepared DS-FCPCM has good solvent resistance. This is attributed to the physical and chemical cross-linked network in the samples, which provides a stable shape while also achieving complete encapsulation. Fig. 5(c) shows photographs of the material undergoing flexural bending at 30 °C. It can be observed that the material still possesses good flexibility when bent close to 90°, forming a highly thermally conductive colloidal structure. This structure gives the material a significant advantage in resisting impact and forming complex shapes, and allows it to fully conform to different surfaces in practical applications, improving energy storage efficiency.

3.5. Dynamic properties

To achieve the goal of creating environmentally friendly materials, DMG was added during the preparation of the DS-FCPCM, leading to the reaction of some of the isocyanate groups (-NCO) on the MDI with the ketoxime groups (-NOH) on the DMG. This resulted in the formation of oxime-urethane bonds alongside the polyurethane chemical cross-linked network. The presence of dynamic oxime-urethane bonds endows the material with self-healing and reprocessability characteristics. To further investigate the dynamic properties of the DS-FCPCM, a thermal healing experiment was designed for verification. As shown in Fig. 6(a), a formed rectangular sheet of DS-FCPCM was divided, and the cut edges were aligned and placed in a drying oven at 60 °C (above the phase transition temperature) for heat treatment. After 6 h of heating, as shown in Fig. 6(b), healing was observed at the cut. As the heating time increased, the cut edges of the sample gradually became uniform and flat, forming a complete sheet. The emergence of this phenomenon fully demonstrates that the DS-FCPCM has strong dynamic properties and reprocessability, achieving the goal of creating environmentally friendly materials.

Fig. 6(c) and (d) presents the tensile stress-strain curves of the materials, where A1c and B1c denote cracked samples A1 and B1, respectively, while A1h and B1h represent their healed counterparts. In the original samples, the A1 specimen with a DS skeleton exhibited a fracture stress of 12.9 MPa and an elongation at break of 954 %, demonstrating an 8.1 % enhancement in tensile strength but a 12.2 % reduction in ductility compared to the DS-free B1 sample. This highlights the role

of the DS network in mediating the stiffness-toughness balance of the material. The fracture stresses of A1c and A1h were 70.23 % and 89.14 % of pristine A1, respectively, with corresponding deformations of 73.90 % and 88.05 %. Similarly, B1c and B1h showed fracture stresses of 64.52 % and 91.93 % of original B1, respectively, with corresponding deformations of 76.03 % and 84.79 %. This comparative analysis suggests that fractured EG undergoes irreversible damage, thus hindering the overall self-healing capability. Fig. 6(e) and (f) displays the thermal conductivity and DSC test results before and after healing. Despite the EG fractures, the material retained its thermal conductivity, as the silica sol-based thermally conductive matrix effectively filled gaps in the EG thermal pathways, maintaining high heat transfer efficiency. Consistent enthalpy values between healed and original specimens indicate that the PEG matrix retained its phase change energy storage capacity during healing. The phase change matrix, PEG, retains a high enthalpy of fusion because its thermal energy storage structure doesn't participate in the chemical reactions involved in the healing process. Remarkably, the DS-FCPCM achieves an 89.14 % self-healing rate [50] while maintaining exceptional mechanical properties: a fracture stress of 12.9 MPa and a deformation capacity approximately 9.5 times that of conventional materials (Table 4 summarises key mechanical parameters of various self-healing materials). This combination of performance metrics surpasses most reported self-healing materials, establishing its superior overall mechanical characteristics.

3.6. Thermal regulation properties

The thermal regulation performance of DS-FCPCM materials is an important parameter for their practical application as energy storage materials. To test this, water bath heating and cooling experiments were designed for verification. As shown in Fig. 7(a), PEG, DS, A1, and B1 samples of equal mass were independently placed in test tubes to form isolated thermal systems. Two thermostatic water baths were set to temperatures of 75 °C and 20 °C (the high temperature exceeding the material's phase change heat absorption temperature and the low temperature falling below the material's phase change heat release temperature) to ensure that the materials experienced a complete phase change process within this temperature range. A multi-channel temperature tester was used to record temperatures at multiple points, with a temperature acquisition rate of 0.5 s per reading. Fig. 7(b) shows the system temperature curves after the materials had undergone 10 thermal cycles. During the phase change heat absorption stage, the DS system curve took 350 s to reach its target temperature, because the presence of expanded graphite and silica sol provided a high overall thermal conductivity for the material. The B1 sample, lacking a DS thermally conductive scaffold, had a relatively lower thermal conductivity, causing the system curve to take 874 s to reach its target temperature. The PEG system curve took 1090 s to reach its target temperature, because the PEG sample had a low thermal conductivity but a relatively high heat storage enthalpy value. The thermal conductivity of the A1 sample was higher than that of B1 but lower than that of DS. Therefore, the heating rate of the A1 system curve was between those of the DS and B1 curves, consuming 516 s, and its thermal response speed was 2.11 times that of PEG. Similarly, due to the different thermal conductivities and enthalpy values, the curve cooling rates during the phase change heat release stage gradually increased in the order B1, PEG, A1, and DS systems. At the same time, the maximum temperature difference between the PEG and A1 systems was 8.1 °C. Fig. 7(c), (d), and (e) show the water bath plots of system temperature changes after 50, 100, and 200 phase change cycles, respectively. These plots are similar to the 10th thermal cycle curves, demonstrating that the heat storage properties of the material did not change after multiple cycles. The specific data are presented in Table 5. The water bath experiment curves correspond with the thermal conductivity and DSC test results mentioned above, further verifying the heat storage properties of the material. The results show that the DS-FCPCM prepared in this study has a fast thermal response speed, good thermal stability, and chemical stability, meeting the usage requirements.

4. Conclusion

In this study, a dynamically self-healing colloidal composite phase change material (DS-FCPCM) was successfully fabricated through physicochemical crosslinking, introducing dynamic oxime-urethane bonds during the encapsulation of polyethylene glycol (PEG). Leveraging the strong adsorption capacity of the expanded graphite-silica sol high-thermal-conductivity skeleton enabled effective encapsulation of the phase change material, PEG. The resultant material exhibits a thermal conductivity of 0.5023 W/(m·K) and a maximum phase change enthalpy of 91.724 J/g. Remarkably, the material maintains excellent thermal storage performance after 200 thermal cycles. Structural characterisation reveals that a dual synergistic mechanism—combining expanded graphite interlayer conduction and silica sol network conduction—establishes an efficient heat transfer pathway. When the ambient temperature exceeds the phase transition temperature, dynamic chemical bonds trigger the reversible reorganization of the crosslinked network. This endows the material with temperature-responsive self-healing capability and reprocessability (exhibiting a 12.9 MPa fracture stress, 954 % elongation at break, and 89.14 % healing efficiency), thereby effectively maintaining structural integrity. Systematic evaluations via differential scanning calorimetry (DSC), thermogravimetric analysis (TG), solvent resistance testing, and leakage experiments confirm the exceptional thermal reliability and environmental stability of DS-FCPCM. This work not only significantly extends the service life of phase change materials through dynamic crosslinking technology but also reduces potential ecological impacts due to enhanced environmental stability, thereby offering novel insights for the development of multifunctional CPCMs.

CRediT authorship contribution statement

Jinbao Zhong: Methodology, Investigation. **Jian Zhang:** Writing – review & editing, Writing – original draft, Formal analysis, Data curation. **Yongpeng Wang:** Supervision. **Haoxi Fan:** Software. **Xiangyi Meng:** Resources. **Xianglong Feng:** Conceptualization. **Jianhang Yan:** Validation.

Declaration of competing interest

The authors declare that they have no known competing financial interests or personal relationships that could have appeared to influence the work reported in this paper.

Data availability

Data will be made available on request.

References

[1] Z. Song, J. Wang, S. Tang, et al., Dual-objective topology optimization design for latent heat storage systems using composite phase change materials, Energy 319 (2025) e135069, https://doi.org/10.1016/j.energy.2025.135069.
[2] A. Tamraparni, J. Rendall, Z. Shen, et al., Experimental investigation on phase change material–based finned tube heat exchanger for thermal energy storage and building envelope thermal management, Appl. Therm. Eng. 273 (2025) e126490, https://doi.org/10.1016/j.applthermaleng.2025.126490.
[3] K.U. Paul, S.M. Mohtasim, G.M. Kibria, et al., Nano-material based composite phase change materials and nanofluid for solar thermal energy storage applications: Featuring numerical and experimental approaches, J. Energy Storage 98 (PB) (2024) e113032, https://doi.org/10.1016/j.est.2024.113032.
[4] A. Faseena F, A. Sreekumar, Advances, perspectives and challenges in phase change material based battery thermal management: A comprehensive review, J. Energy Storage 113 (2025) e115644, https://doi.org/10.1016/j.est.2025.115644.
[5] W. Fu, J. Lao, L. Chen, et al., Design of Na2HPO4·12H2O/diatomite composite phase change materials with low supercooling degree, excellent thermal properties

and corrosion resistance for building energy conservation, J. Energy Storage 84 (PA) (2024) e110922, https://doi.org/10.1016/j.est.2024.110922.
[6] L. Wei, L. Shuoya, Z. Kaiyu, et al., Experimental and numerical study on temperature control performance of phase change material heat sink, Appl. Therm. Eng. 238 (2024) e122081, https://doi.org/10.1016/j.applthermaleng.2023.122081.
[7] L. Jiang, X. Ma, C. Yang, et al., Preparation of HDA/DHPD/EG composite phase change materials with stable morphology and good thermal performance for low-temperature waste heat recovery by demulsification, Ceram. Int. 50 (19PB) (2024) 36174–36184, https://doi.org/10.1016/j.ceramint.2024.07.002.
[8] T. Wang, J. Deng, J. Du, et al., Investigation on the polyethylene glycol based composite phase change materials with coating flame-retardant for battery thermal management, Case Stud. Therm. Eng. 65 (2025) e105616, https://doi.org/10.1016/j.csite.2024.105616.
[9] S.R. Ferfera, B. Madani, A. Kouidri, Experimental investigation on convective heat transfer of heat sink based on paraffin/copper foam composite material, J. Energy Storage 119 (2025) e116347, https://doi.org/10.1016/j.est.2025.116347.
[10] Y. Gao, H. Liu, H. Gui, et al., Solid-liquid phase change materials microcapsules: Synthesis strategies, thermal storage and beyond, Prog. Nat. Sci. Mater. Int. 34 (4) (2024) 615–631, https://doi.org/10.1016/j.pnsc.2024.06.011.
[11] J. Ji, Y. An, J. Gu, et al., Flexible composite phase change materials with high thermal conductivity and electrical insulation properties for lithium-ion battery thermal management, Appl. Therm. Eng. 266 (2025) e125706, https://doi.org/10.1016/j.applthermaleng.2025.125706.
[12] Y. Yang, C. Liu, Y. Shi, et al., Intrinsic photothermal block polyurethane solid–solid phase-change materials with high mechanical toughness and multi-recyclability controlled by crosslinking density, J. Energy Storage 113 (2025) e115583, https://doi.org/10.1016/j.est.2025.115583.
[13] X. Dai, P. Ping, D. Kong, et al., Experimental investigation on flexible inorganic phase change material for thermal management performance improvement of lithium-ion battery, Appl. Therm. Eng. 272 (2025) e126358, https://doi.org/10.1016/j.applthermaleng.2025.126358.
[14] S. Xin, M. Sun, S. Liu, et al., Preparation and properties of low-exothermic polyurethanes doped with modified hydrated salt phase change materials, Molecules 30 (7) (2025) 1508, https://doi.org/10.3390/molecules30071508.
[15] S.R. Calolsa, T. Sumangala, K.S. Kalpathy, et al., Development of a novel PDMS/PEG/PDMS multilayered composite film for advanced thermal management solutions for photovoltaics, Mater. Lett. 390 (2025) e138421, https://doi.org/10.1016/j.matlet.2025.138421.
[16] Y. Li, T. Wang, J. Zhang, et al., Multi-mode triggered bio-based epoxy resin/lauric acid/graphene paper flexible phase change materials with high enthalpy value, multi-functionality, and personal thermal management ability, Compos. Part A Appl. Sci. Manuf. 193 (2025) e108849, https://doi.org/10.1016/j.compositesa.2025.108849.
[17] B. Ai, Z. Liu, X. Hu, et al., Sandwich-structured HDPE-based medium-temperature phase change composites with MXene interlayers for photo-thermal-electrical applications, Chem. Eng. J. 512 (2025) e162367, https://doi.org/10.1016/j.cej.2025.162367.
[18] Y. Pang, J. Chen, J. Sun, et al., A flexible phase change composite encapsulated in cellulose nanofiber/ polyacrylamide layered porous structure for thermal energy storage and management, Ind. Crop. Prod. 222 (P4) (2024) e119920, https://doi.org/10.1016/j.indcrop.2024.119920.
[19] S. Liu, H. Zhang, X. Zhang, et al., Reversible thermochromic microencapsulated phase change materials with silane-terminated polyurethane shell, J. Energy Storage 119 (2025) e116329, https://doi.org/10.1016/j.est.2025.116329.
[20] Z. Jianhua, L. Geng, N. Zhuanli, et al., Hyperbranched waterborne polyurethane solid–solid phase change material for thermal energy storage in thermal management fabric, Fibers Polym. 24 (2) (2023) 413–422, https://doi.org/10.1007/s12221-023-00081-3.
[21] R. Huang, A. Yang, Z. Liu, et al., Poly(ethylene glycol)-based polyurethanes based on dynamic oxime-urethane bonds for sustainable thermal energy storage, Colloids Surf. A Physicochem. Eng. Asp. 698 (2024) e134544, https://doi.org/10.1016/j.colsurfa.2024.134544.
[22] X. Zhang, F. Dong, M. Yu, et al., Multifunctional waterborne polyurethane-cellulose nanofiber composite: Realizing ultrarobust, photoluminescence and swift self-healing via multi-dynamic bonding, Chem. Eng. J. 507 (2025) e160302, https://doi.org/10.1016/j.cej.2025.160302.
[23] J. Yao, W. Nie, et al., BaTiO3/polyurethane dielectric composites with Diels-alder bond for improved self-healing properties, J. Renewable Mater. 10 (9) (2022) 2355–2364, https://doi.org/10.32604/jrm.2022.019339.
[24] D.B. Goteti, B S, R.P. Kumar, Thermally remendable bismalemide-MWCNT/DA-epoxy nanocomposite via Diels-alder bonding, Polymer 245 (2022) e124734, https://doi.org/10.1016/j.polymer.2022.124734.
[25] H. Xu, R. Zhai, Z. Hao, et al., A facile strategy for multiple dynamic polyurethane with high mechanical strength, room-temperature healability and recoverability, React. Funct. Polym. 211 (2025) e106216, https://doi.org/10.1016/j.reactfunctpolym.2025.106216.
[26] K. Dong, D. Zhao, Y. Pang, et al., Multiple-reprocessable guaiacol-derived epoxy vitrimer with disulfide crosslinks and closed-loop recycling of carbon fiber-reinforced composites, Chem. Eng. J. 508 (2025) e160754, https://doi.org/10.1016/j.cej.2025.160754.
[27] F. Wei, Y. Wu, M. Li, et al., Hydrogen bond cross-linked photo-healable multifunctional phase change materials for thermal management, J. Energy Storage 106 (2025) e114821, https://doi.org/10.1016/j.est.2024.114821.
[28] Y. Hang, J. Chenming, Y. Hua, Photothermal self-healing polyurethane/graphene oxide composites based on diselenide bond, Polym. Test. 117 (2023) e107813, https://doi.org/10.1016/j.polymertesting.2022.107813.
[29] T.M. Tamás, A. M, L. Łukasz, et al., Facile modification of hydroxyl group containing macromolecules provides autonomously self-healing polymers through the formation of dynamic Schiff base linkages, Eur. Polym. J. 168 (2022) e111086, https://doi.org/10.1016/j.eurpolymj.2022.111086.
[30] W. Fan, Y. Jin, L. Shi, et al., Developing visible-light-induced dynamic aromatic Schiff base bonds for room-temperature self-healable and reprocessable waterborne polyurethanes with high mechanical properties, J. Mater. Chem. A 8 (2020) 6757–6767, https://doi.org/10.1039/C9TA13928A.
[31] Z. Kang, G. Qingbao, S. Wei, et al., Hot-melt adhesive based on dynamic oxime-carbamate bonds, Ind. Eng. Chem. Res. 60 (19) (2021) 6925–6931. https://pubs.acs.org/doi/10.1021/acs.iecr.1c00768.
[32] C. Yingchao, L. Chunmei, Y. Yumin, et al., Self-healable and reprocessable cross-linked poly(urea-urethane) elastomers with high mechanical performance based on dynamic oxime-carbamate bonds, Ind. Eng. Chem. Res. 60 (37) (2021) 13585–13593. https://pubs.acs.org/doi/10.1021/acs.iecr.1c02245.
[33] S. Jiaxin, Z. Tianze, Z. Yao, et al., Cross-linked polyurethane with dynamic phenol-carbamate bonds: Properties affected by the chemical structure of isocyanate Dagger, Polym. Chem. 12 (16) (2021) 2421–2432, https://doi.org/10.1039/D1PY00157D.
[34] H. Jin, Y. Ruhan, Z. Li, et al., Robust, transparent, and self-healable polyurethane elastomer via dynamic crosslinking of phenol-carbamate bonds, Polymer 222 (2021) e123674, https://doi.org/10.1016/j.polymer.2021.123674.
[35] P. Xu, N. Ding, H. Wang, et al., Synergistic cross-linking strategy with oxime-carbamate and hydrogen bonding arrays for excellent damage self-healing and reprocess ability of thermoset polyurethanes, Chem. Eng. J. 508 (2025) e160951, https://doi.org/10.1016/j.cej.2025.160951.
[36] X. Wang, L. Wang, C. Liu, et al., Self-healing polyurethane elastomers with superior tensile strength and elastic recovery based on dynamic oxime-carbamate and hydrogen bond interactions, Macromol. Rapid Commun. 45 (13) (2024) e2400022, https://doi.org/10.1002/marc.202400022.
[37] G. Wang, L. Liu, X. Hu, et al., Aerogel-functionalized phase change materials toward lightweight and robust thermal management, Small Methods (2025) e2500127, https://doi.org/10.1002/smtd.202500127.
[38] J. Yang, B.A. Ali, A.A.M.Y. Zahy, et al., The effect of copper oxide nanoparticles on the thermal behavior of silica aerogel/paraffin as a phase change material in a cylindrical channel with molecular dynamics simulation, Prog. Nucl. Energy 181 (2025) e105645, https://doi.org/10.1016/j.pnucene.2025.105645.
[39] H. Hu, C. Wang, S. Xie, et al., Polyethylene glycol/carboxymethyl cellulose/montmorillonite composite phase change materials for thermal management, J. Energy Storage 105 (2025) e114714, https://doi.org/10.1016/j.est.2024.114714.
[40] S. Liu, W. Gao, J. Deng, et al., Capric-lauric & capric-palmitic/modified bentonite composite as phase change materials for thermal energy storage, J. Energy Storage 99 (PA) (2024) e113315, https://doi.org/10.1016/j.est.2024.113315.
[41] X. Gu, F.G. Huseien, T. Kar, et al., Hazelnut shell-based activated carbon/carbon nanotubes/palmityl alcohol as new form-stable phase change material with enhanced energy storage capacity and thermal conductivity, J. Energy Storage 103 (PB) (2024) e114346, https://doi.org/10.1016/j.est.2024.114346.
[42] S.S. K, Abanti S, Ground tire rubber/activated carbon/expanded graphite aerogels and foams as support material for the preparation of polyethylene glycol composite phase change materials for thermal energy storage applications, J. Energy Storage 78 (2024) e109805, https://doi.org/10.1016/j.est.2023.109805.
[43] H. Jia, S. Lu, W. Wu, et al., Synthesis and thermal properties of sodium acetate trihydrate-based composite phase change materials with modified expanded graphite, Journal of Energy Storage 113 (2025) e115628, https://doi.org/10.1016/j.est.2025.115628.
[44] J. Zhao, Y. Chen, M. Chen, Battery thermal management with a modified metal alloy/expanded graphite/paraffin composite phase change material, J. Energy Storage 113 (2025) e115652, https://doi.org/10.1016/j.est.2025.115652.
[45] Y. Dongmao, M. Weixing, L. Song, et al., Polyethylene glycol (PEG)/silicon dioxide grafted aminopropyl group and carboxylic multi-walled carbon nanotubes (SAM) composite as phase change material for light-to-heat energy conversion and storage, J. Energy Storage 36 (2021) e102428, https://doi.org/10.1016/j.est.2021.102428.
[46] L. Wang, L. Ye, X. Cheng, et al., Shape-stabilized polyethylene glycol composite phase change materials based on dendritic mesoporous silica sphere support for thermal energy storage, Sol. Energy Mater. Sol. Cells 282 (2025) e113425, https://doi.org/10.1016/j.solmat.2025.113425.
[47] Y. Yang, B. Liu, T. Zhang, et al., Improved design, analysis, preparation and properties of photothermal phase-change polyurethane materials based on zinc ion coordination, Prog. Org. Coat. 201 (2025) 109098, https://doi.org/10.1016/j.porgcoat.2025.109098.
[48] W. Jiao, J. Zhang, Z. Zhang, et al., Development of PTMEG/MDI-based solid-solid phase change materials for asphalt pavements deicing, Constr. Build. Mater. 467 (2025) e140301, https://doi.org/10.1016/j.conbuildmat.2025.140301.
[49] R. Huang, A. Yang, R. Ma, et al., Polyurethane solid-solid phase change materials based on triple dynamic bonds with excellent mechanical and self-healing

properties for sustainable thermal energy storage, J. Energy Storage 111 (2025) e115447, https://doi.org/10.1016/j.est.2025.115447.
[50] S. Parasuram, S. Tripathi, R.M. Jain, et al., Dual dynamic CAN and graphene oxide offer unique synergism in improving mechanical properties and introducing self-healing in carbon fiber composites, Composites Part A 195 (2025) e108959, https://doi.org/10.1016/j.compositesa.2025.108959.
[51] C. Xiaojing, Q. Xiaolin, F. Xiaoyue, et al., Temperature-sensitive and self-healing shape-stable phase change materials containing temperature adjustable ionic liquid for improving the recycling stability and the applicability in cold energy storage, J. Energy Storage 68 (2023) e107722, https://doi.org/10.1016/j.est.2023.107722.

Glossary

PEG: Polyethylene Glycol
DS: Expanded graphite-silica sol composite scaffold
DS-FCPCM: Dual-Scaffold Flexible Composite Phase Change Material
DBTDL: Dibutyltin Dilaurate
EG: Expanded Graphite
SNOWTEX: Silica Sol
DPE: Dipentaerythritol
THF: Tetrahydrofuran
DMG: Butanedione dioxime
KH550: 3-Aminopropyltriethoxysilane
DMF: N,N-Dimethylformamide
MDI: Methylene diphenyl diisocyanate
FTIR: Fourier transform infrared spectroscopy
XRD: X-ray diffraction
DSC: Differential scanning calorimetry
TG: Thermogravimetric Analysis